

Article

Magnetic Properties of Nanosized Fe and FeCo Systems on Trenched Mo Templates

Anda Elena Stanciu ^{1,*}, Gabriel Schinteie ¹, Andrei Cristian Kuncser ¹, Claudiu Locovei ^{1,2},
Lucian Trupina ¹, Nicusor Iacob ¹, Aurel Leca ¹, Bogdana Borca ¹ and Victor Kuncser ^{1,*}

¹ National Institute of Materials Physics, Atomistilor 405A, 077125 Magurele, Romania

² Faculty of Physics, University of Bucharest, Atomistilor 405, 077125 Magurele, Romania

* Correspondence: anda.stanciu@infim.ro (A.E.S.); kuncser@infim.ro (V.K.)

Abstract: The manipulation of magnetic anisotropy represents the fundamental prerequisite for the application of magnetic materials. Here we present the vectorial magnetic properties of nanostructured systems and thin films of Fe and FeCo prepared on linearly trenched Mo templates with thermally controlled periodicity. The magnetic properties of the nanosystems are engineered by tuning the shape, size, thickness, and composition parameters of the thin films. Thus, we control coercivity, magnetization, orientation of the easy axis of magnetization, and the long-range magnetic order of the system in the function of the temperature. We distinguish magnetic components that emerge from the complex morpho-structural features of the undulating Fe or FeCo nanostructured films on trenched Mo templates: (i) assembly of magnetic nanowires and (ii) assembly of magnetic islands/clusters. Uniaxial anisotropy at room temperature was proven, characterized, and explained in the case of all systems. Our work contributes to the understanding of magnetic properties necessary for possible further applications of linear systems and undulated thin films.

Keywords: magnetic anisotropy; linear nanostructures; Fe; FeCo; Mo; structured template



Citation: Stanciu, A.E.; Schinteie, G.; Kuncser, A.C.; Locovei, C.; Trupina, L.; Iacob, N.; Leca, A.; Borca, B.; Kuncser, V. Magnetic Properties of Nanosized Fe and FeCo Systems on Trenched Mo Templates. *Coatings* **2022**, *12*, 1366. <https://doi.org/10.3390/coatings12091366>

Academic Editor: Igor V. Khudiyakov

Received: 8 August 2022

Accepted: 14 September 2022

Published: 19 September 2022

Publisher's Note: MDPI stays neutral with regard to jurisdictional claims in published maps and institutional affiliations.



Copyright: © 2022 by the authors. Licensee MDPI, Basel, Switzerland. This article is an open access article distributed under the terms and conditions of the Creative Commons Attribution (CC BY) license (<https://creativecommons.org/licenses/by/4.0/>).

1. Introduction

Modern spintronic applications demand nanosized systems (thin films, nanowires, and nanoparticles) that should satisfy several conditions regarding the magnetic properties and magnetic anisotropy. They should present controllable magnetic properties, such as the value of the magnetic anisotropy energy, saturation magnetization, the relative orientation of the easy axis of magnetization of nano-objects, coercivity, and squareness factor. Also, the possibility to switch the magnetization with low-cost external stimuli and to stabilize the magnetic states upon exposure to thermal fluctuations or external fields is required [1–4].

Depending on the application type, the magnetic anisotropy should be either in plane or out of plane. For example, in the case of high-density magnetic recording and high-frequency magnetic devices perpendicular magnetic anisotropy is needed. The in-plane magnetic anisotropy with uniaxial anisotropy is used in random access memory devices and in the hard disk drive head component [5]. Otherwise, an in-plane isotropically coercive free layer allowing stabilizing the magnetization in any direction between the parallel and the antiparallel magnetic configurations, is proposed for efficient spintronic memristive applications [6–9]. In these cases, the intermediate resistance states in between the maximum and the minimum values corresponding to the parallel and antiparallel alignment of the magnetization of top and bottom layers sandwiching a conductive/isolating thin spacers are obtained via the dependence of the giant/tunneling magnetoresistance on the angle between the magnetization directions of the two magnetic layers of different magnetic anisotropies.

Tuning the magnetic anisotropy can be achieved via a series of different preparation methods and conditions. Morpho-structural aspects and structured topography obtained

for example by ion beam etching and wet chemical etching [6], oblique deposition [8–10] or applying a magnetic field during deposition [11], can be exploited with the purpose to pattern the magnetic material. External control of magnetic anisotropy, coercivity, or magnetic relaxation/superparamagnetism can be achieved via the application of an electric field [12,13]. A different choice is to achieve in-plane uniaxial magnetic anisotropy that may be obtained in a common way by organizing matter into linear objects with a small dimensionality for example nanowires, stripes, and nanotubes with regular shape and spacing [2,3] or by depositing magnetic systems on valley's deeps of undulated surfaces [14]. Moreover, nanowires and linear systems can be implemented in a wide range of applications in domains such as electronics [15], photonics [16,17], sensoristics [18], or thermoelectrics [19].

A way of preparing nanowires, stripes, and linear structures is based on using pre-engineered substrates to guide the growth. A major advantage of this method is the possibility of producing ordered arrays with a narrow size distribution of the component entities [20]. Thus, self-assembled magnetic monoatomic wires could be obtained on a vicinal surface [21] or on faceted surfaces with controllable periodicity [22,23]. Besides, the angular distribution of the easy axis of magnetization corresponding to the magnetic system and its overall anisotropy can be tuned from an almost uniaxial (Dirac-like angular distribution) to an almost isotropic one (random-like angular distribution) [24].

In the present work, we are following a method that supposes the use of a nanostructured surface with linearly faceted trenches as a template [22,23]. The trenches can be obtained by homoepitaxy of a refractory metal (W or Mo) with body-centered cubic crystalline structure, deposited on a nominal planar surface.

The lateral periodicity of the trenches, which are mainly oriented in the [001] crystallographic direction, can be controlled kinetically by tuning the deposition temperature [25]. We were using Mo for the formation of trenches because it favors the in-plane anisotropy with an easy axis along the trenches ([001] direction) in the case of Fe films deposited on Mo [25–27]. Magnetic nanostructures were subsequently engineered as undulated thin films of Fe and FeCo by deposition on the faceted trenches of the substrate, with the aim to control the magnetic properties and especially the magnetic anisotropy. Here we compare the magnetic properties of an undulated Fe film with those of a FeCo film with similar effective thicknesses given the possibility to tune the coercive field and the saturation magnetization of Fe intermetallic compounds by Co addition [28]. The influence of composition, effective thickness, and shape effects were considered. The wetting particularities of the deposited materials were proven to have also an important role. Accordingly, different types of nanostructures of Fe and FeCo with a distribution of the easy axis of magnetization from in-plane isotropic to uniaxial anisotropic, without or with out-of-plane components, were obtained. These systems have promising applications for memristive devices [5]. On the other hand, studying the magnetic properties of an undulated FeCo film from a fundamental point of view is motivated by the rich specificities the magnetic FeCo or Fe/Co systems exhibit such as magnetostriction [29], magnetoresistance [30], or hosting topological textures known as skyrmions [31]. We revised the magnetic properties of Fe and FeCo undulated thin films with limiting cases (defined by geometrical structure aspects) such as: (i) assembly of magnetic nanowires and (ii) assembly of magnetic islands/clusters.

2. Materials and Methods

The samples were prepared in an ultra-high vacuum (the base pressure was 1×10^{-9} Torr) by Magnetron Sputtering deposition on mono-crystalline Al_2O_3 sapphire substrates with (11 $\bar{2}$ 0) crystal orientation, acquired from CrysTec GmbH. The thickness of the deposited materials was estimated in-situ with a quartz crystal microbalance and the results were corroborated with post-deposition interferometry and profilometry measurements realized ex-situ. In order to obtain optimal deposition conditions for the realization of the desired structures the following parameters have been adjusted: the pressure of the working gas (Ar), the value of the power used, applying RF or DC voltage, the substrate temperature

during deposition or the thermal treatment temperature after deposition. The Mo trenches were obtained by depositing in the first step a Mo layer under a power of 7–9 W in DC, for 20–25 min at RT. In order to obtain sequences of trenches with different periodicity [22], two sets of temperature intervals were used during the homoepitaxial growth of Mo/Mo/Al₂O₃: 500–280 °C and 300–180 °C, respectively. In a second step, a Mo layer was deposited with 9 W in DC for 60 min. Magnetic layers of Fe and, respectively, FeCo were realized by deposition at 175 °C from corresponding unique targets, with a DC power of 20 W for 6 min and 15 W for 6.5 min, respectively. On trenches of higher lateral periodicity, we deposited a FeCo film in the same conditions as the previously described FeCo sample. A thicker sample of FeCo depositing under a DC power of 7 W for 60 min was grown also on Mo trenches of higher lateral periodicity. The low DC power used for Mo, Fe, and FeCo (e.g., 1 Å/min for Mo and 2 Å/min for Fe) sputtering allowed for achieving very low deposition rates that are required to obtain small crystallites [28]. The obtained magnetic nanostructures were covered with a 2–5 nm thick Mo layer to prevent oxidation processes.

Morpho-structural and compositional characterization were mainly realized via microscopic measurements using Atomic Force Microscopy (AFM) and Transmission Electron Microscopy (TEM). Atomic force microscopy (AFM) was performed using an MFP 3D SA (Asylum Research, Oxford Instruments, Santa Barbara, United States) microscope. Surface topography images for 1 mm square scan areas were obtained by tapping (or AC or non-contact) mode using commercial Si cantilevers (AC160TS, spring constant $k = 26$ N/m and resonance frequency $f = 275$ kHz, Olympus Co. Ltd., Shinjuku, Tokyo, Japan). Transmission Electron Microscopy (TEM) measurements have been performed using a Cs-corrected JEOL ARM 200F instrument (JEOL Ltd., Akishima, Tokyo, Japan) with Electron Energy Loss Spectroscopy (EELS) capabilities. TEM specimens have been prepared using the standard cross-sectional method, involving mechanical polishing followed by ion polishing using the PIPS (Precision Ion Polishing System) system (GATAN Inc., Pleasanton, United States). TEM was also used in the mass thickness contrast mode. Vectorial magnetic measurements were realized using room temperature longitudinal Magneto-Optical Kerr Effect (MOKE) investigating the magnetic properties at different orientations of the applied field in the sample plane. Temperature-dependent magnetic properties were analyzed by Superconducting Quantum Interference Device (SQUID) magnetometry between 10 and 300 K, applying a magnetic field in two directions in the sample plane (longitudinal and transversal geometry) and perpendicular to the sample plane (perpendicular geometry).

3. Results

3.1. Structural and Morphological Investigations of Fe Linear Structures

As described in Refs. [20,21,23], Mo faceted linear structures with [001] crystallographic orientation can be prepared, this direction being favored at Mo/Fe interfaces as the easy axis of magnetization of Fe. Following similar deposition conditions, even some differences may occur due to the use here of a different deposition method [32–35], firstly a 5 nm thick Mo film was deposited on an Al₂O₃ and it was thermally treated after deposition, in order to obtain a planar flat surface. Then, a Mo layer having a thickness of 15 nm was re-deposited on the planar Mo surface while varying the deposition temperature, in order to obtain the arrays of linearly trenched structures [22]. For all samples, we used these structures as a template for the growth of Fe and FeCo thin films. AFM, TEM images, and sketches of representative samples are presented in Figure 1. The AFM images correspond to planar atomic surfaces of the Al₂O₃ substrate (Figure 1a) and to the first wetting Mo layer (Figure 1b). Linear patterns observed in the approximately diagonal direction of the image represent atomic steps corresponding to the Al₂O₃ substrate with an average periodicity of 35 nm, followed by the first thermal treated Mo layer. Figure 1c shows the profiles of the structures over the lines presented in the two images. Beyond the AFM resolution, trenches were evidenced by TEM. In Figure 1d the TEM images (inset: chemical contrast) in the profile plane of a Fe sample with a nominal thickness of approximately

3 nm and lateral periodicity of trenches of approximately 15 nm are shown. Fe molds on the structured Mo surface and accumulates deep inside the trenches.

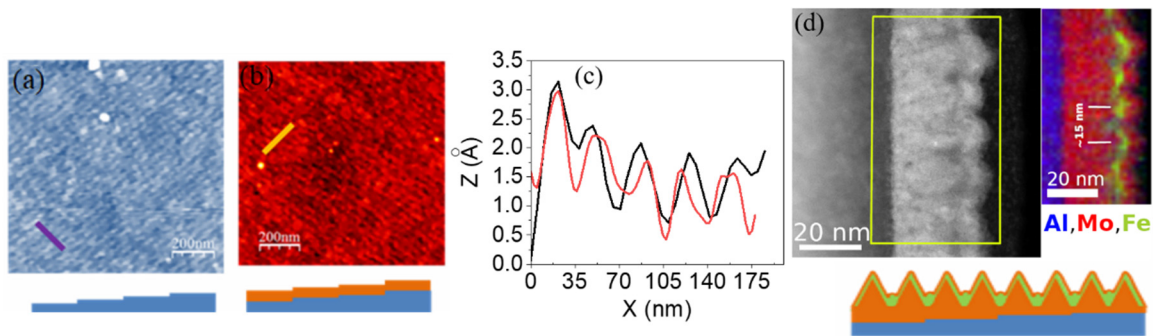


Figure 1. Microscopic images of the linear systems with the corresponding schematic representation in the lower part of the figure. (a) AFM image of the planar surface of Al_2O_3 substrate with atomic terraces of 35 nm average periodicity. (b) AFM image of the wetting layer of Mo surface following the structure of the Al_2O_3 substrate that was used for the deposition of the template presenting Mo linear trenches. (c) Topographic profiles realized over the lines marked in (a,b). (d) TEM image and the elemental spectroscopic analysis (inset) in a profile plane of a Fe sample prepared by deposition on Mo trenches. The sample is covered with a thin Mo layer against oxidation processes.

3.2. Magnetic Characterization

Usually, two types of magnetic measurements are performed for the characterization of the nanosystems: (i) hysteresis loops for the investigation of the magnetic reversal mechanisms and (ii) specific measurements of zero-field-cooling—field-cooling (ZFC-FC) procedures for the investigation of the magnetic relaxation mechanisms. The measuring geometry for the vectorial investigation of the magnetization reversal depends on the orientation of the applied magnetic field and will be defined as follows according to the inset of Figure 2a: (i) longitudinal, with the magnetic field applied along O_z direction (along the wave), (ii) transversal, with the magnetic field applied along the O_x direction (perpendicular to the wave, but in the film plane) and (iii) perpendicular, with the magnetic field applied along to the O_y direction (perpendicular to the film plane).

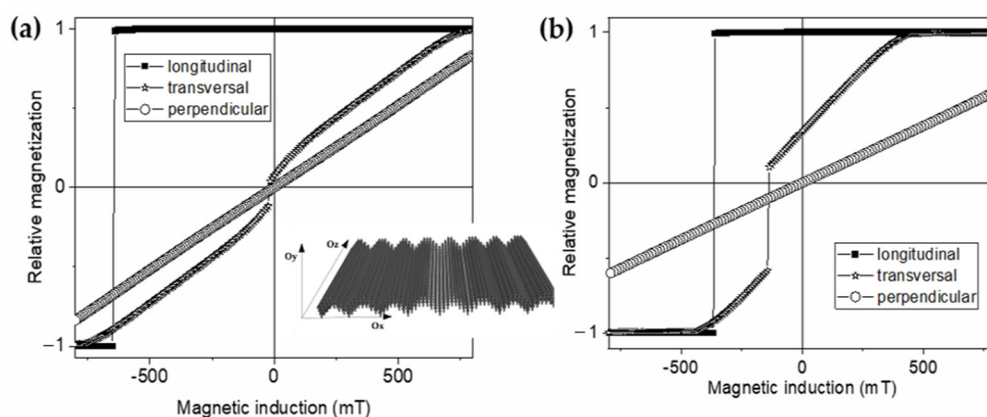


Figure 2. The magnetization reversal of an undulated Fe thin film with a thickness of 3 nm, deep of the valley of 5 nm, and lateral periodicity of 15 nm, in case of three specific directions of the applied magnetic field. The considered geometry with the associated reference system used in the computations is shown in the inset (a). The magnetization reversal of an undulated Fe thin film with a thickness of 3 nm, deep of the valley of 3 nm, and lateral periodicity of 15 nm, for the same three specific measurement geometries (b).

According to the present samples, three types of nanostructures should be critically revised: (i) assembly of magnetic nanowires, (ii) assembly of magnetic islands/clusters, and

(iii) undulated magnetic films. However, depending on the undulated film characteristics (lateral periodicity, deep and longitudinal uniformity) the last system can cover at the limit the first two cases, as well as the case of a quasi-uniform thin film. For example, undulated templates with deep well-formed trenches of high lateral periodicity and very low thickness of the magnetic film can lead to non-interacting filiform/quasi-cylindrical nanowires. Specific magnetization reversal mechanisms depend on the nanowire diameter [36,37]. If the lateral periodicity is decreased, the assembly of nanowires that interact by dipolar magnetic interactions is obtained [38]. If the longitudinal uniformity of the nanowires is lost, separate segments of nanowires of different aspect ratios (nanocluster-like) are obtained [39]. Depending on the separation gap and the transversal periodicity, such clusters can interact along the chain (unidimensional magnetic systems) as well as between chains (bi-dimensional magnetic systems). Moreover, depending on the shape and size of the magnetic clusters, they can become superparamagnetic above a certain temperature [40]. Depending on the wetting conditions and type of magnetic materials, a very broad distribution of magnetic clusters (both in size and aspect ratio) can be formed along the trenches. If the inter-chain magnetic interaction is mediated by the finest clusters which become superparamagnetic above a certain temperature, a unidimensional magnetic system is expected above this temperature and a bi-dimensional one, below. Magnetic relaxation and blocking temperatures of possible magnetic clusters can be observed in this case by typical ZFC-FC measurements.

In order to interpret the magnetic measurements of the prepared systems, firstly theoretical expectations on the magnetization reversal mechanism obtained by micromagnetic simulations will be briefly discussed in the case of some ideal systems derived from undulated magnetic thin films. The magnetization reversal of an undulated Fe thin film with a thickness of 3 nm, deep of the valley of 5 nm, and lateral periodicity of 15 nm is shown in Figure 2a. The simulations have been performed using the OOMMF (Object Oriented Micromagnetic Framework) public domain software, developed by the Applied and Computational Mathematics Division of National Institute of Standards and Technology (NIST) [41]. The considered geometry and the discretization space are presented in the inset. Half of the loops (from the highest positive applied magnetic field to the highest negative field) are shown. The three-magnetization reversal effects presented in Figure 2 correspond to the three above-mentioned directions of the applied magnetic field: (i) field applied along the wave (longitudinal geometry), (ii) field applied perpendicular to the wave but in the film plane (transversal geometry) and (iii) field applied perpendicular to the film plane (perpendicular geometry).

In longitudinal geometry, it is observed the typical jump of the relative magnetization (current magnetization relative to the spontaneous magnetization which can be experimentally approximated by saturation magnetization at low temperatures) from 1 to -1 , specific to a magnetization reversal with the field applied along a magnetic easy axis. In this case, the easy axis is along the wave (Oz axis). On the other hand, the magnetization reversal in perpendicular geometry is linearly increasing with the applied field, according to a coherent spin rotation typical to a hard magnetic axis. Finally, in transversal geometry, the magnetization reversal approaches well a coherent spin rotation, except for a narrow interval of low fields (order of magnitude lower than the switching/jumping field in longitudinal geometry) where a fast reorientation of the spins take place. The situation is not similar to a magnetic field applied perpendicular to a narrow angular distribution of easy axes due to the rectangular shape of the loop in longitudinal geometry (field applied along the easy axis). Moreover, due to the lower value of the switching field in longitudinal geometry with respect to the saturation field in perpendicular geometry (that means with the film applied along an easy and hard axis of magnetization), the magnetization reversal mechanism in undulated thin films has to be represented by magnetic walls displacement anywhere a switching field is evidenced (e.g., in both longitudinal and transversal geometry) [36,40]. At variance to the film with a deep of the valley of 5 nm where the switching field in longitudinal geometry is about 6000 Oe, in the case of the film with a lateral periodicity

of 15 nm and deep of the valley of 3 nm, the switching field in longitudinal geometry is about 4000 Oe whereas in transversal geometry the jump in magnetization is larger and at a switching field closer to the switching field in longitudinal geometry. At the same time, the coherent rotation in perpendicular geometry develops much harder (i.e., lower magnetic susceptibility) than in the former case. To note that in a planar geometry (0 nm deep of the valley), with in plane magnetic anisotropy, a full magnetization reversal from 1 to -1 appears at the same very low field of order of hundred Oe in both longitudinal and transversal geometries whereas the coherent reversal is the hardest. At this point, one may conclude on undulated thin films of Fe (and by extension of any soft ferromagnetic film) that the magnetic reversal mechanism depends not only on the direction of the magnetic field with respect to the structuring wave, but also on the wave characteristics with respect to the film thickness. In the case of a lateral periodicity of about 15 nm as in the present case, for nanometer-sized valley deeps larger than the film thickness, a strong in-plane uniaxial anisotropy (shape related) with the easy axis along the waves is evidenced by micromagnetic calculations. The magnetization reversal in longitudinal geometry takes place at a switching field higher than a few thousand Oe, via a fast domain wall displacement. In transversal geometry (with the field applied along the film but perpendicular to the wave), a coherent rotation takes place initially, followed by a final switching by domain wall displacement in lower negative fields of the order of hundred Oe. The coherent spin rotation which is in work in perpendicular geometry is saturated in fields higher than 10 kOe. By decreasing the valley deep down to the film thickness, the discrepancies between the magnetic reversal loops in longitudinal and transversal geometries become lower and lower, involving however almost similar switching fields of the order of kOe. The saturation of the coherent spin rotation in perpendicular geometry becomes harder and harder, involving applied magnetic fields of many tenths of kOe.

Besides, the magnetization reversal of magnetic clusters depends on both the size and the shape of the clusters. Ellipsoidal magnetic nanoparticles of enough low size and aspect ratio with magnetic monodomain structure can be superparamagnetic above the blocking temperature whereas below the blocking temperature the magnetization reversal respects the Stoner-Wohlfarth mechanism [41]. Rectangular hysteresis loops are obtained with the field applied along the easy axis, the switching field being dependent on the shape anisotropy energy and taking values of hundreds of Oe in the case of ellipsoidal Fe and FeCo nanoparticles of high aspect ratios. A coherent spin rotation takes place with the magnetic field applied perpendicular to the easy axis with the saturation field equating to the switching field. Given the trenched structure of the template, ellipsoidal magnetic nanostructures may be dominantly formed in case of unappropriated wetting of the deposited material. In fact, this limiting case can be obtained starting also from the unidirectional case of filiform configurations along the trenches. Accordingly, in the peculiar case of undulated templates with trenches of high lateral periodicity, non-interacting filiform nanowires (deposited only in the valley) can be obtained for the deposited effective thickness of the film lower than half of the deep of the valley. The magnetization reversal of the assembly respects the magnetization reversal of a nanowire, which is strongly dependent on its diameter. Coherent rotation behavior (Stoner-Wohlfarth like) is specific to nanowires of soft magnetic materials (Ni, Fe, and even Co) with diameters lower than 4–5 nm whereas for higher diameters other mechanisms are in work (transverse wall mode, curling mode, etc.). However, in all cases a distinction can be made in the reversal loops obtained with the applied field along the easy axis (longitudinal geometry in the present case) and perpendicular to the easy axis (either transversal geometry or perpendicular geometry in the present case). Rectangular loops are specific to longitudinal geometry and linear ones to transversal and perpendicular geometries (with saturation field equating to the switching field in case of only coherent rotation and a higher saturation field than the switching field in case of transverse wall mode). If dipolar interactions take place between the nanowires, deviations from both the rectangular and linear variation of the magnetization versus field may appear. Such much-rounded shapes of the loops can be

also due to local discontinuities of the nanowires, leading to the distribution of magnetic segments, easily associated with a distribution of ellipsoidal nanoparticles of different sizes and aspect ratios.

Moreover, before the presentation of the experimental vectorial magnetic reversal curves depending on the direction of the applied magnetic field with respect to sample-related fixed axes, it is worth mentioning some important specificities for its interpretation. There are well-known pitfalls of SQUID measurements in the case of magnetic measurements on non-uniform magnetic configurations of extremely low magnetic moments [42,43]. It was proved that due to different filling factors of the SQUID pick-up coils, large variation in the measured signal (e.g., the total magnetic moment at saturation) can be observed depending on the orientation of the sample with respect to the coil geometry (such discrepancies are even more evident in case of nanostructures grown on diamagnetic substrates). Usually, the pick-up coils are concentric to the superconducting coil which generates the applied magnetic field, and hence the measured signal will depend on the orientation of the magnetic structure with respect to the field. Therefore, not the values of the saturation magnetization in different geometries will be critically discussed, but the overall vectorial behavior (the shape) of the hysteresis loops at different orientations of the applied field with respect to the nanostructured samples. It should be noted that the diamagnetic contribution of the substrate was properly subtracted in the case of the hysteresis loops presented in the next sections.

3.2.1. Magnetic Characterization of Fe Undulated Systems (with an Effective Thickness of 3 nm) Deposited on Mo Trenches

Magnetic properties of Fe nanostructures, with a thickness of 3 nm—as derived from the TEM image (Figure 1d), i.e., the magnetic anisotropy, the magnetic moment, and the easy axis of magnetization are determined from the observed magnetic behavior at various orientation of the applied field versus sample plane and a fixed in-plane direction as well as at different temperatures. Magnetic hysteresis loops acquired at 10 K and at different orientations of the applied field with respect to the structured undulated plane, as well as at different temperatures are presented in Figures 3a and 3b respectively.

Neglecting the values of the saturation magnetization (due to the pitfalls of such specific SQUID measurements) two main observations should be underlined from Figure 3a: (i) rounded hysteresis loops of similar shapes and coercive fields of about 280 Oe are obtained in transversal and longitudinal geometry at 10 K (no dominant easy axis specific to strongly undulated thin films) and (ii) a relative fast saturation within a not opened loop in perpendicular geometry. According to the above discussion, the only situation for such a behavior can be explained by a quasi-discontinuous undulated thin film formed by three-dimensional islands of Fe of nanometer size (about 5 nm), which strongly interact at low temperature. Hence, at 10 K, the magnetization reversal will be specific to a combination between the long-range magnetic structure of an undulated thin film with an equivalent thickness higher to the valley deep (with negligible difference between magnetization reversal in transversal and longitudinal geometry) and an assembly of quasi-spheroidal nanoparticles which open the low coercive loop specific to the magnetic frozen state below the blocking temperature. As a consequence, due to nanoparticle-related components, the similar reversal loops in longitudinal and transversal geometries will present a relatively low coercive field as compared to a simple undulated thin film whereas. Also, the magnetic reversal in perpendicular geometry will present a higher magnetic susceptibility in low fields, followed by an apparent saturation due to the compensation of the diamagnetic susceptibility of the substrate with the positive susceptibility of the undulated film.

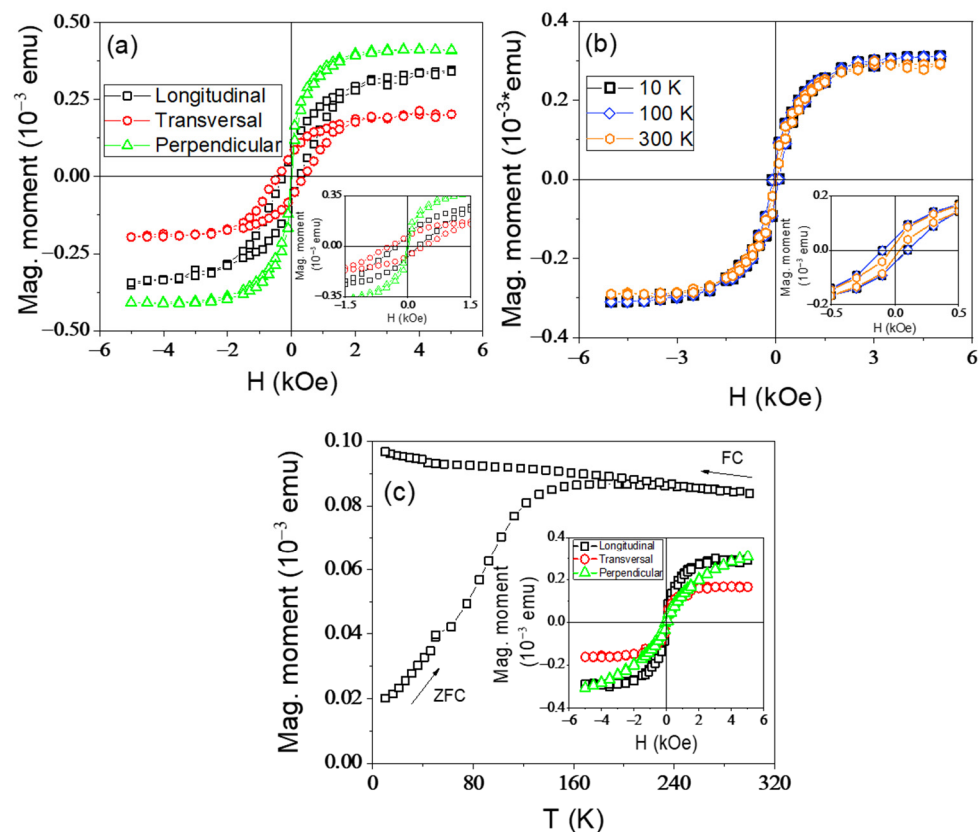


Figure 3. Hysteresis loops of the Fe nanostructured system collected at 10 K in longitudinal, transversal, and perpendicular geometry (a); hysteresis loops as a function of temperature in longitudinal geometry (b). Insets present an enlarged image of the hysteresis loops around the origin. ZFC-FC curves collected with 200 Oe applied field in longitudinal geometry. Inset shows the hysteresis loops collected at 300 K in different geometries (c).

By increasing the temperature, the finest nanoclusters (smallest Fe islands) become progressively superparamagnetic, canceling the interactions between the larger clusters. As a consequence, the long-range magnetic order specific to the undulated thin film structure disappears and the coercive field in the longitudinal magnetization reversal (specific to only an assembly of non-interacting magnetic nanoparticles) decreases progressively with the temperature while more and more nanoparticles become superparamagnetic (Figure 3b). This behavior is also nicely supported by the ZFC-FC curves presented in Figure 3c. The ZFC-FC procedure was carried out by measuring the magnetic signal with an applied magnetic field of 200 Oe while increasing temperature, after the previous cooling of the sample in a null magnetic field. As the temperature is increased, a progressive increase of the magnetic moment is observed due to a size distribution of the magnetic entities (and implicitly of the magnetic moment) as a consequence of their deblocking followed by their orientation towards the applied field. The range of temperatures at which the magnetic moment is increasing corresponds to the distribution of sizes of the magnetic entities and thus, of the blocking temperature. An average blocking temperature of about 136 K (in longitudinal geometry) was estimated at the maximum of zero-field cooling (ZFC) curves. From the variation of the coercive fields in Figure 3b with the \sqrt{T} a final blocking temperature of about 150 K was determined. Despite the large error in the determination of this value due to the lack of experimental points, it is in good agreement with the blocking temperature estimated from the ZFC-FC curves. To note the very slow decrease of the curves above the branching point, proving a very broad size distribution of the Fe islands in the film. The magnetic moment measured at room temperature supports also the existence of magnetically frozen nanoparticles even at room temperature.

3.2.2. Magnetic Characterization of FeCo Undulated Systems (with an Effective Thickness of about 3 nm) Deposited on Mo Trenches

For comparison, a FeCo sample was prepared in the same experimental conditions as the Fe undulated system characterized above, keeping the same effective thickness of 3 nm of the FeCo magnetic layer. Magnetic reversal loops measured in different geometries and at different temperatures are presented in Figure 4a,b. There is not a notable difference between the magnetization reversal loops collected at 10 K with the field applied in the sample plane (longitudinal, transversal, and oblique geometries, the last one meaning the field oriented at 45 degrees with respect to longitudinal and transversal direction), similar to the previous case. The coercive field is in this case about 200 Oe (so, slightly lower than in the case of the Fe film), inferring on one hand an undulated long-range magnetic structure with an effective thickness higher than the valley deep, and on the other hand, rather the formation of oblate FeCo islands/nanoparticles (e.g., with lateral sizes larger than the highness). As a consequence, the magnetic susceptibility in perpendicular geometry is much lower in the case of the FeCo oblate nanoparticles/spheroids than in the case of the quasi-spheroidal Fe ones, and therefore, the overall contribution to the magnetic susceptibility at 10 K coming from the undulated FeCo thin film with long-range magnetic order, the system of FeCo oblate nanoparticles in the magnetic frozen regime and the diamagnetic substrate becomes negligible. This is an additional reason for the very low values of magnetization over the whole range of applied magnetic fields during the magnetic reversal in perpendicular geometry. On the other hand, the evolution of the coercive field with temperature in longitudinal geometry is quite similar to the one of the 3 nm Fe film. Following the same explanation, the finest FeCo oblate nanoparticles become superparamagnetic at higher temperatures (as proven also by the ZFC-FC measurements in Figure 4c), canceling out the long-range magnetic interaction of the non-homogeneous undulated FeCo thin film. The magnetic behavior is due to only the assembly of non-interacting FeCo nanoparticles which enter progressively the superparamagnetic state at a higher temperature.

The blocking temperature estimated from the ZFC curve measured in longitudinal geometry with an applied field of 200 Oe is about 157 K (Figure 4c). The insignificant decrease of magnetization above the branching temperature infers also FeCo nanoparticles of large size and shape distribution, many particles remaining in the blocked state also at room temperature. However, the larger blocking temperature and coercive field in longitudinal geometry in the case of the FeCo system as compared to the Fe system, give support for an in-plane anisotropy of the largest nanoparticles, higher in the case of FeCo systems. Nevertheless, this situation becomes possible only for quasi-ellipsoidal nanoparticles (prolate spheroids) oriented along the trenches. Hence, a higher in-plane uniaxial anisotropy of the system can be kept at 300 K (easy axis along the ellipsoidal nanostructures) in the FeCo systems. Given this behavior, two FeCo systems grown on trenches of higher periodicity will be considered, with the aim of diminishing the lateral dipolar interaction between the ellipsoidal nanoparticles which are magnetically blocked at room temperature.

3.2.3. Magnetic Characterization of FeCo Nanostructured System (with a Thickness of 3 nm) Deposited on Mo Trenches Prepared at Higher Temperature Than Those Presented in Section 3.2.2

Considering a further possibility to control the magnetic properties of these nanosystems, we prepared Mo templates using a temperature gradient in the range (500–200 °C), which induces a larger periodicity than that of the first two samples [22]. These templates were used for the deposition of FeCo films of two different effective thicknesses.

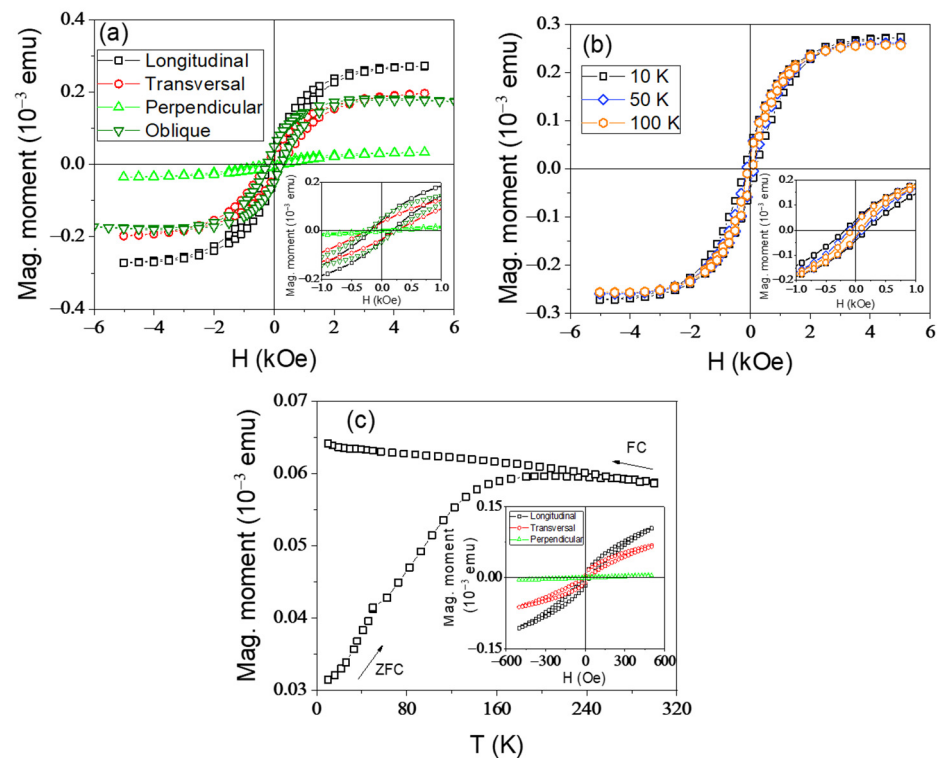


Figure 4. Hysteresis loops of FeCo sample collected at 10 K in longitudinal, transversal, oblique, and perpendicular geometry (a); hysteresis loops as a function of temperature in longitudinal geometry (b). Insets present an enlarged image of the hysteresis loops around the origin. ZFC-FC curves collected with 200 Oe applied field in longitudinal geometry. Inset shows the hysteresis loops collected at 300 K in different geometries (c).

Hysteresis loops were collected at 10 K in different geometries and at different temperatures and the ZFC-FC curves of the FeCo system with the same thickness (3 nm) and deposition conditions similar to the one presented in Section 3.2.2, are shown in Figure 5. However, in this case, the faceted template should have a higher periodicity of the trenches than the previous system. If concerning the magnetization reversal in longitudinal and transversal geometries the situation is similar to of the previous FeCo film (with almost the same shape and a coercive field of 200 Oe in both geometries), a significant difference appears in the perpendicular geometry (Figure 5a). This behavior might be induced by the Co composites and the magnetization reversal mechanism that is strongly dependent on the geometrical configuration of the finest FeCo nano-islands/nanoparticles which are blocked at low temperature and assure the long-range magnetic interaction of the undulated film and develops along a more rounded hysteresis loop, of high coercive field. The only explanation for this behavior, is the formation of oblate islands/spheroids grown on the wave side, in such a way that a field perpendicular to the undulated film will make a small but finite angle with the plane of the quasi-bidimensional island. According to the Stoner-Wohlfarth model, the magnetization reversal develops in this case gradually (with low magnetic susceptibility), but with a sensible coercive field. By increasing the temperature, the finest FeCo nanoparticles become superparamagnetic, cutting out the interaction among the largest prolate islands (nanoparticles assimilated to prolate spheroids with the long axis along trenches. Accordingly, the coercive field of the assembly of non-interacting prolate nanoparticles decreases with temperature, as the effect of more and more nanoparticles entering the superparamagnetic regime (Figure 5b), similar to the case of the previous FeCo film. However, the ZFC-FC curves, in this case, suggest a much-increased blocking temperature above 300 K (Figure 5c), meaning longer prolate magnetic nanostructures along the trenches.

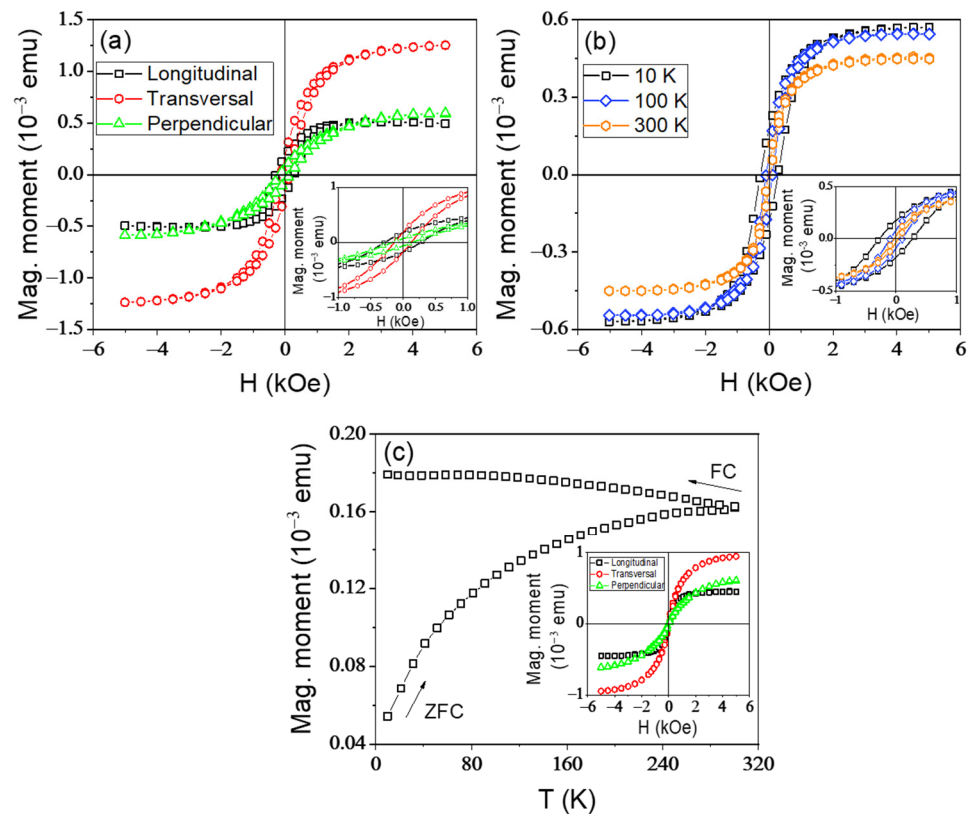


Figure 5. Hysteresis loops of a 3 nm FeCo film grown on more distanced trenches, collected at 10 K in longitudinal, transversal, and perpendicular geometry (a); hysteresis loops as a function of temperature in longitudinal geometry (b). Insets present an enlarged image of the hysteresis loops around the origin; ZFC-FC curve in longitudinal geometry. Inset shows the hysteresis loops collected at 300 K in different geometries (c).

3.2.4. Magnetic Characterization of a Thicker FeCo System than the One Presented in Section 3.2.3

In order to further study the influence of the film thickness on the magnetic properties of such nanostructures, a much thicker FeCo system of approximately 15 nm (5 times higher thickness than the systems presented above) was prepared on Mo linear trenches. The grooved Mo templates were deposited at a temperature gradient of (500–300 °C) similarly to the system previously presented. Hysteresis loops collected at 10 K in different geometries and at different temperatures as well as the specific ZFC-FC curves are illustrated in Figure 6. A noticeable difference can be observed in Figure 6a as compared to Figure 5a. That is the higher coercive field (800 Oe as compared to 200 Oe) reflected by the two loops of similar shape collected in longitudinal and transversal geometry. That means the undulated thin film contribution to the in-plane anisotropy of the system becomes dominant over the oblate nanoislands grown on the wave side, as will be easily expected from the deposition of a thicker film. On the contrary, in the perpendicular geometry where the spins of the undulated film respond very hardly to the field, the dominant increase of magnetization is given by the magnetization reversal of the finest oblate nanoislands which are magnetically frozen at low temperature and hence the shape of the loop is similar to the previous case. At increasing temperature, the finest oblate nanoparticles become superparamagnetic and cancel out the long-range magnetic interaction between larger clusters, leading to magnetic configurations specific to undulated thin films. Hence, the coercive field of the assembly of the prolate nanoclusters decreases at increasing temperatures due to the increased number of superparamagnetic nanoparticles/nanoislands (Figure 6b). The average blocking temperature, well above 300 K as deduced from the ZFC-FC curves

presented in Figure 6c is even higher than in the previous case, proving the formation of prolate nanoislands of higher aspect ratio (or anisotropy constant).

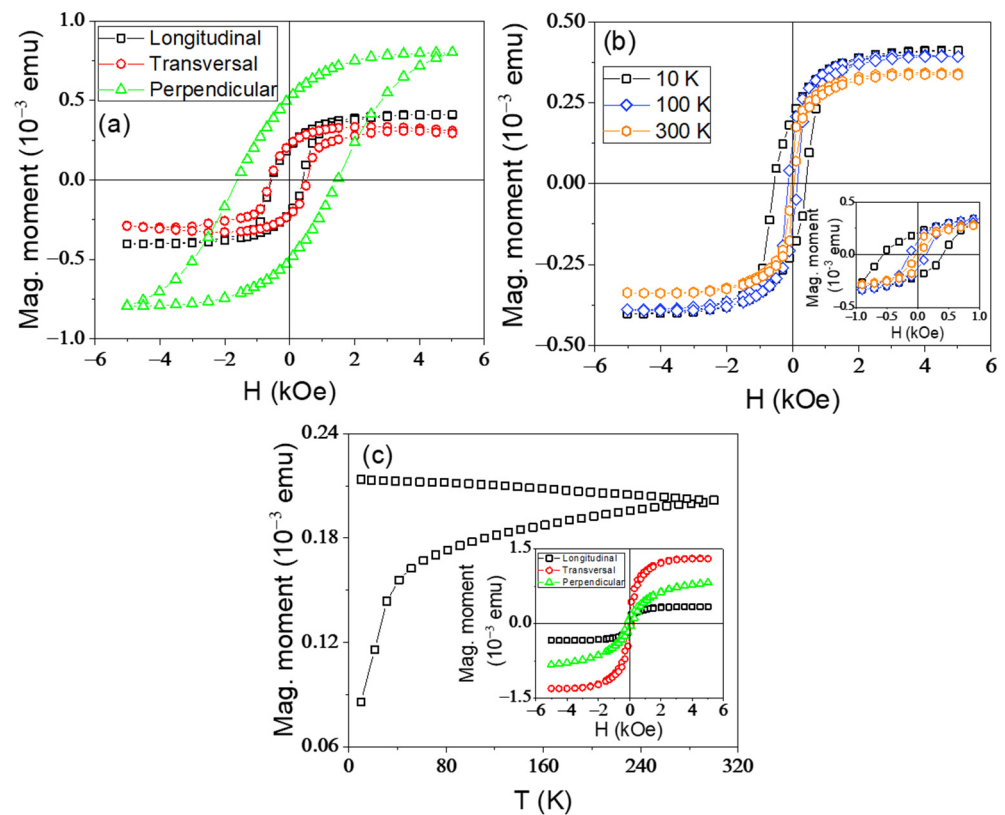


Figure 6. Hysteresis loops of 15 nm FeCo film grown on more distanced trenches, collected at 10 K in longitudinal, transversal, and perpendicular geometry (a); hysteresis loops as a function of temperature in longitudinal geometry (b). Insets present an enlarged image of the hysteresis loops around the origin. ZFC-FC curve in longitudinal geometry. Inset shows the hysteresis loops collected at 300 K in different geometries (c).

Due to the higher effective thickness of the inhomogeneous FeCo film, the in-plane magnetic properties of the FeCo system were also characterized at room temperature by magneto-optical measurements using a MOKE magnetometer.

Specific vectorial hysteresis loops (at different orientations of the field with respect to the trenches direction), as well as polar representations of the relative remnant magnetization (remnant to saturation magnetization ratio) and of the normalized coercive field (current coercive field reported to the maximal coercive field) obtained from the MOKE hysteresis loops collected at different azimuthal angles, are shown in Figure 7. The ample variation of the shape of the hysteresis loops with the azimuthal angle, translated also in the large oscillations of both the relative remnant magnetization and normalized coercive field, proves clearly the high uniaxial anisotropy of the system along the trenches achieved at room temperature in such systems.

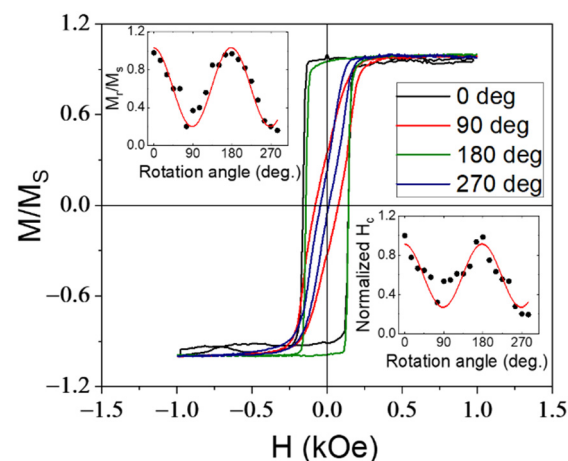


Figure 7. MOKE loops of FeCo structures with a thickness of 15 nm deposited on Mo with linear trenches, collected at different azimuthal angles with respect to the direction of trenches; Angular representation of the relative remanent magnetization and normalized coercive field are shown in insets.

4. Conclusions

Nanostructured undulated thin films of Fe and FeCo were prepared on trenched Mo templates. We characterize the vectorial magnetic properties by tuning the shape, size, thickness, and composition parameters of the system. Inhomogeneous undulated thin films consisting of low size oblate islands and larger prolate islands with the magnetic easy axis along the trenches were obtained in all cases. Both the long-range magnetic ordered undulated system and the nanoparticulate system contribute to the magnetization reversal at low temperatures. By increasing the temperature, the low-size oblate nanoparticles become superparamagnetic and cut off the long-range interactions among the larger prolate nanoparticles. Hence, at room temperature, the magnetization reversal is specific to an assembly of non-interacting oblate ellipsoidal nanoparticles which behave as nanowires with the easy axis of magnetization oriented along the trenches. The uniaxial anisotropy of the system at room temperature and the complex anisotropy at low temperature can be controlled by induced specificities of trenches, thickness, and composition of the magnetic material. The obtained results open new paths for the extension of the studies concerning the adjustment of magnetic properties on various linear magnetic systems and thin films.

Author Contributions: Conceptualization, B.B., G.S. and V.K.; methodology, investigation, and data curation A.E.S., B.B., G.S., A.C.K., C.L., L.T., N.I. and A.L.; writing—original draft preparation, A.E.S., B.B. and V.K.; writing—review and editing, B.B. and V.K.; visualization, A.E.S. and B.B.; supervision, B.B. and V.K.; project administration, B.B. and V.K.; funding acquisition, A.E.S., B.B. and V.K. All authors have read and agreed to the published version of the manuscript.

Funding: This work was supported by the Romanian Ministry of Research and Innovation through projects: Core Program PN19 (Contract No. 21N/2019), PN-III-P1-1.2-PCCDI-2017-0152 (contract no. 75PCCDI/2018), PN-III-P2-2.1-PED-2021-0378 (contract no. 575PED/2022) and PN-III-P1-1.1-PD-2019-1141 (contract no. PD 163/2020). The research leading to these results has also received funding from the NO-RO grants 2014–2021, under Project contract No 39/2021.

Institutional Review Board Statement: Not applicable.

Informed Consent Statement: Not applicable.

Data Availability Statement: Not applicable.

Acknowledgments: The authors thank Cristian Mihail Teodorescu for support coordinating the 75PCCDI/2018 project. The authors acknowledge Daniel Bürgler from Research Center Jülich (FZJ) for making possible the use of test substrates.

Conflicts of Interest: The authors declare no conflict of interest.

References

1. Guimarães, A.P. Magnetism of Thin Films and Multilayers. In *Principles of Nanomagnetism*, 1st ed.; Springer: Berlin/Heidelberg, Germany, 2009; Volume 7, pp. 112–117.
2. Dorantes-Dávila, J.; Pastor, G.M. Magnetic Anisotropy of One-Dimensional Nanostructures of Transition Metals. *Phys. Rev. Lett.* **1998**, *81*, 208–211. [[CrossRef](#)]
3. Staño, M.; Fruchart, O. Magnetic nanowires and nanotubes. In *Handbook of Magnetic Materials*, 1st ed.; Elsevier: Amsterdam, The Netherlands, 2018; Volume 2, pp. 155–267.
4. Bhatti, S.; Sbiaa, R.; Hirohata, A.; Ohno, H.; Fukami, S.; Piramanayagam, S.N. Spintronics based random access memory: A review. *Mater. Today* **2017**, *20*, 530–548. [[CrossRef](#)]
5. Mansueto, M.; Chavent, A.; Auffret, S.; Joumard, I.; Nath, J.; Miron, I.M.; Ebels, U.; Sousa, R.C.; Buda-Prejbeanu, L.D.; Prejbeanu, I.L.; et al. Realizing an Isotropically Coercive Magnetic Layer for Memristive Applications by Analogy to Dry Friction. *Phys. Rev. Appl.* **2019**, *12*, 44029. [[CrossRef](#)]
6. Buddea, T.; Gatzert, H.H. Thin film SmCo magnets for use in electromagnetic microactuators. *J. Appl. Phys.* **2006**, *99*, 08N304. [[CrossRef](#)]
7. Mansueto, M.; Chavent, A.; Auffret, S.; Joumard, I.; Vila, L.; Sousa, R.C.; Buda-Prejbeanu, L.D.; Prejbeanu, I.L.; Dieny, B. Spintronic memristors for neuromorphic circuits based on the angular variation of tunnel magnetoresistance. *Nanoscale* **2021**, *13*, 11488–11496. [[CrossRef](#)]
8. Pan, L.; Wang, F.; Wang, W.; Chai, G.; Xue, D. In-plane Isotropic Microwave Performance of CoZr Trilayer in GHz Range. *Sci. Rep.* **2016**, *6*, 21327. [[CrossRef](#)]
9. Ali, Z.; Basaula, D.; Eid, K.F.; Khan, M. Anisotropic properties of oblique angle deposited permalloy thin films. *Thin Solid Films* **2021**, *735*, 138899. [[CrossRef](#)]
10. Li, J.; Zhan, Q.; Zhang, S.; Wei, J.; Wang, J.; Pan, M.; Xie, Y.; Yang, H.; Zhou, Z.; Xie, S.; et al. Magnetic anisotropy and high-frequency property of flexible FeCoTa films obliquely deposited on a wrinkled topography. *Sci. Rep.* **2017**, *7*, 2837. [[CrossRef](#)]
11. Cao, D.; Zhu, Z.; Feng, H.; Pan, L.; Cheng, X.; Wang, Z.; Wang, J.; Liu, Q. Applied magnetic field angle dependence of the static and dynamic magnetic properties in FeCo films during the deposition. *J. Magn. Magn. Mater.* **2016**, *416*, 208–212. [[CrossRef](#)]
12. Terada, H.; Ohya, S.; Anh, L.D.; Iwasa, Y.; Tanaka, M. Magnetic anisotropy control by applying an electric field to the side surface of ferromagnetic films. *Sci. Rep.* **2017**, *7*, 5618. [[CrossRef](#)]
13. Lau, Y.-C.; Sheng, P.; Mitani, S.; Chiba, D.; Hayashi, M. Electric field modulation of the non-linear areal magnetic anisotropy energy. *Appl. Phys. Lett.* **2017**, *110*, 022405. [[CrossRef](#)]
14. Sánchez, E.H.; Rodríguez-Rodríguez, G.; Aragón, R.; Arranz, M.A.; Rebollar, E.; Castillejo, M.; Colino, J.M. Anisotropy engineering of soft thin films in the undulated magnetic state. *J. Magn. Magn. Mater.* **2020**, *514*, 167149. [[CrossRef](#)]
15. Lu, W.; Lieber, C.M. Nanoelectronics from the bottom up. *Nat. Mat.* **2007**, *6*, 841–850. [[CrossRef](#)] [[PubMed](#)]
16. Pauzauskis, P.; Yang, P. Nanowire photonics. *Mater. Today* **2006**, *9*, 36–45. [[CrossRef](#)]
17. Arranz, M.A.; Sánchez, E.H.; Rebollar, E.; Castillejo, M.; Colino, J.M. Form and magnetic birefringence in undulated Permalloy/PET films. *Opt. Express* **2019**, *27*, 21285–21294. [[CrossRef](#)]
18. Patoisky, F.; Lieber, C. Nanowire nanosensors. *Mater. Today* **2005**, *8*, 20–28. [[CrossRef](#)]
19. Chen, R.; Lee, J.; Lee, W.; Li, D. Thermoelectrics of nanowires. *Chem. Rev.* **2019**, *119*, 9260–9302. [[CrossRef](#)]
20. Rousset, S.; Croset, B.; Girard, Y.; Prévot, G.; Repain, V.; Rohart, S. Self-organized epitaxial growth on spontaneously nanopatterned templates. *C. R. Phys.* **2005**, *6*, 33–46. [[CrossRef](#)]
21. Gambardella, P.; Dallmeyer, A.; Maiti, K.; Malagoli, M.C.; Eberhardt, W.; Kern, K.; Carbone, C. Ferromagnetism in one-dimensional monatomic metal chains. *Nature* **2002**, *416*, 301–304. [[CrossRef](#)]
22. Borca, B.; Fruchart, O.; Cheynis, F.; Hasegawa, M.; Meyer, C. Growth and magnetism of self-organized arrays of Fe (110) wires formed by deposition on kinetically grooved W (110). *Surf. Sci.* **2007**, *601*, 4358–4361. [[CrossRef](#)]
23. Borca, B.; Fruchart, O.; Kritsikis, E.; Cheynis, F.; Rousseau, A.; David, P.; Meyer, C.; Toussaint, J.C. Tunable magnetic properties of arrays of Fe (1 1 0) nanowires grown on kinetically grooved W(1 1 0) self-organized templates. *J. Magn. Magn. Mater.* **2010**, *322*, 257–264. [[CrossRef](#)]
24. Kuncser, A.; Kuncser, V. Magnetization reversal via a Stoner–Wohlfarth model with bi-dimensional angular distribution of easy axis. *J. Magn. Magn. Mater.* **2015**, *395*, 34–40. [[CrossRef](#)]
25. Borca, B.; Fruchart, O.; David, P.; Rousseau, A.; Meyer, C. Kinetic self-organization of trenched templates for the fabrication of versatile ferromagnetic nanowires. *Appl. Phys. Lett.* **2007**, *90*, 142507. [[CrossRef](#)]
26. Fruchart, O.; Nozieres, J.P.; Givord, D. Growth and interface magnetic anisotropy of epitaxial Mo/Fe/Mo (1 1 0) and W/Fe/W (1 1 0) ultrathin films. *J. Magn. Magn. Mater.* **1999**, *207*, 158–167. [[CrossRef](#)]
27. Prokop, J.; Kukunin, A.; Elmers, H.J. Magnetic anisotropies and coupling mechanisms in Fe/Mo (110) nanostripes. *Phys. Rev. Lett.* **2005**, *95*, 187202. [[CrossRef](#)]
28. Kishimoto, M.; Latiff, H.; Kita, E.; Yanagihara, H. Morphology and magnetic properties of FeCo particles synthesized with different compositions of Co and Fe through co-precipitation, flux treatment, and reduction. *J. Magn. Magn. Mater.* **2019**, *476*, 229–233. [[CrossRef](#)]

29. Beato-López, J.J.; Urdániz-Villanueva, J.G.; Pérez-Landazábal, J.I.; Gómez-Polo, C. Giant stress impedance magnetoelastic sensors employing soft magnetic amorphous ribbons. *Materials* **2020**, *13*, 2175. [[CrossRef](#)]
30. Tekgül, A.; Şahin, T.; Köçkar, H.; Alper, M. Structural, magnetic and GMR properties of FeCo (Cu)/Cu magnetic multilayers electrodeposited at high cathode potentials of the magnetic layer. *Optoelectron. Adv. Mater. Rapid Commun.* **2020**, *14*, 189–195.
31. Satywali, B.; Kravchuk, V.P.; Pan, L.; Raju, M.; He, S.; Ma, F.; Petrović, A.P.; Garst, M.; Panagopoulos, C. Microwave resonances of magnetic skyrmions in thin film multilayers. *Nat. Commun.* **2021**, *12*, 1909. [[CrossRef](#)]
32. Chan, K.Y.; Teo, B.S. Investigation into the influence of direct current (DC) power in the magnetron sputtering process on the copper crystallite size. *Microelectron. J.* **2007**, *38*, 60–62. [[CrossRef](#)]
33. Sasaki, T.; Koshizaki, N.; Beck, K.M. Comparison of Pt=TiO₂ nanocomposite films prepared by sputtering and pulsed laser deposition. *Appl. Phys. A* **1999**, *69*, S771–S774. [[CrossRef](#)]
34. Sun, L.; He, J.; Chen, Y.; Yue, F.; Yang, P.; Chu, J. Comparative study on Cu₂ZnSnS₄ thin films deposited by sputtering and pulsed laser deposition from a single quaternary sulfide target. *J. Cryst. Growth* **2012**, *361*, 147–151. [[CrossRef](#)]
35. Le, M.-T.; Sohn, Y.-U.; Lim, J.-W.; Choi, G.-S. Effect of Sputtering Power on the Nucleation and Growth of Cu Films Deposited by Magnetron Sputtering. *Mater. Trans.* **2010**, *51*, 116–120. [[CrossRef](#)]
36. Kuncser, A.; Antohe, S.; Kuncser, V. A general perspective on the magnetization reversal in cylindrical soft magnetic nanowires with dominant shape anisotropy. *J. Magn. Magn. Mater.* **2017**, *423*, 34–38. [[CrossRef](#)]
37. Costas, A.; Florica, C.; Matei, E.; Toimil-Molares, M.E.; Stavarache, I.; Kuncser, A.; Kuncser, V.; Enculescu, I. Magnetism and magnetoresistance of single Ni–Cu alloy nanowires. *Beilstein J. Nanotechnol.* **2018**, *9*, 2345–2355. [[CrossRef](#)]
38. Matei, E.; Enculescu, I.; Toimil-Molares, M.E.; Leca, A.; Ghica, C.; Kuncser, V. Magnetic configurations of Ni–Cu alloy nanowires obtained by the template method. *J. Nanopart. Res.* **2013**, *15*, 1863. [[CrossRef](#)]
39. Locovei, C.; Radu, C.; Kuncser, A.; Iacob, N.; Schinteie, G.; Stanciu, A.; Iftimie, S.; Kuncser, V. Relationship between the Formation of Magnetic Clusters and Hexagonal Phase of Gold Matrix in AuxFe_{1-x} Nanophase Thin Films. *Nanomaterials* **2022**, *12*, 1176. [[CrossRef](#)]
40. Kuncser, V.; Palade, P.; Kuncser, A.; Greculeasa, S.; Schinteie, G.; Kuncser, V. *Size Effects in Nanostructures*; Kuncser, V., Miu, L., Eds.; Springer Series in Materials Science; Springer: Berlin/Heidelberg, Germany, 2014; p. 205.
41. Donahue, M.J.; Porter, D.G. *OOMMF User's Guide, Version 1.0, Interagency Report, NISTIR 6376*; National Institute of Standards and Technology: Gaithersburg, MD, USA, 1999.
42. Stamenov, P.; Coey, J.M.D. Sample size, position, and structure effects on magnetization measurements using second-order gradiometer pickup coils. *Rev. Sci. Instr.* **2006**, *77*, 015106. [[CrossRef](#)]
43. Buchner, M.; Hofler, K.; Henne, B.; Ney, V.; Ney, A. Basic principles, limits of detection, and pitfalls of highly sensitive SQUID magnetometry for nanomagnetism and spintronics. *J. Appl. Phys.* **2018**, *124*, 161101. [[CrossRef](#)]